Journal of Rock Mechanics and Geotechnical Engineering 14 (2022) 494–504

Contents lists available at ScienceDirect

Journal of Rock Mechanics and Geotechnical Engineering

journal homepage: www.jrmge.cn

Full Length Article

Attenuation characteristics of impact-induced seismic wave in deep tunnels: An in situ investigation based on pendulum impact test

Jian Wu [a,b,**], Quansheng Liu [b,c], Xiaoping Zhang [b,c,*], Chuiyi Zhou [a], Xin Yin [b,c], Weiqiang Xie [b,c], Xu Liang [d], Jiaqi Huang [a]

[a] PowerChina Huadong Engineering Corporation Limited, Hangzhou, 311122, China
[b] Key Laboratory of Safety for Geotechnical and Structural Engineering of Hubei Province, School of Civil Engineering, Wuhan University, Wuhan, 430072, China
[c] State Key Laboratory of Water Resources and Hydropower Engineering Science, Wuhan University, Wuhan, 430072, China
[d] Hangzhou Urban Infrastructure Construction Management Center, Hangzhou, 310009, China

ARTICLE INFO

Article history:
Received 10 December 2020
Received in revised form
9 November 2021
Accepted 21 December 2021
Available online 30 December 2021

Keywords:
Attenuation characteristics
Microseismic monitoring
Pendulum impact facility
Seismic energy
Deep tunnels

ABSTRACT

The radiated seismic energy is an important index for the intensity assessment of microseismic (MS) events and the early warning of dynamic disasters. However, the energy of MS signals is significantly attenuated due to the heterogeneity and viscous damping of rock media. Therefore, the study on attenuation characteristics of MS signals in underground engineering has practical significance for the accurately estimation of radiated seismic energy. Based on a pendulum impact test facility and MS monitoring system, an in situ investigation was carried out to explore attenuation characteristics at a deep tunnel. The results show that the seismic energy and peak particle velocity (PPV) attenuation are exponentially related to the propagation distance. The attenuation coefficient of energy is larger than that of PPV. With the increase in the input impact-energy, the seismic energy attenuation coefficient decreases as a power function. An empirical relationship between energy attenuation coefficient and wave impedance of rock mass was established in this scenario. Moreover, the time-frequency characteristics and energy distribution laws of impact-induced signals were investigated by the continuous wavelet transform (CWT) and wavelet packet analyses, respectively. The dominant frequency of signals decreases gradually as the propagation distance increases. Based on the energy attenuation characteristics, a new method was proposed to calculate the released source energy of MS events in the field. This study can provide an insight into energy attenuation characteristics of seismic waves and references for attenuation correction in seismic energy calculation.

1. Introduction

Microseismic (MS) monitoring technique has recently become an effective and applicable method to forecast the hazard of rockbursts in underground engineering (Cai et al., 2001; Trifu and Shumila, 2010; Mazaira and Konicek, 2015; Glazer, 2016; Lu et al., 2018; Li et al., 2021), such as deep tunnels (Feng et al., 2012; Li et al., 2012; Liu et al., 2020; Liang et al., 2020), underground caverns (Chen et al., 2015; Ma et al., 2015; Dai et al., 2016; Z.L Li et al., 2020) and mines (Mendecki, 1997; Urbancic and Trifu, 2000; Snelling et al., 2013). The source parameters of the recorded MS events can be processed to evaluate the evolution of rockbursts, e.g. seismic energy, seismic moment, apparent stress and energy index (Mendecki, 1997; Glazer, 2016; Dai et al., 2016). One of the most important parameters to quantify the intensities of MS events is the radiated seismic energy. However, when an MS signal propagates from the hypocenter to sensors, the energy of MS signal will be significantly attenuated due to the heterogeneity and viscous damping of rock masses. The magnitudes of energy loss are closely associated with the properties of rock masses and geological structures on the propagation path. Therefore, to estimate the seismic energy, it is significant to study the in situ attenuation characteristics of MS signals.

Extensive field investigations have been carried out to study the attenuation characteristics in different geological conditions

* Corresponding author. Key Laboratory of Safety for Geotechnical and Structural Engineering of Hubei Province, School of Civil Engineering, Wuhan University, Wuhan, 430072, China.
** Corresponding author. PowerChina Huadong Engineering Corporation Limited, Hangzhou, 311122, China
E-mail addresses: wu_j23@hdec.com (J. Wu), jxhkzhang@163.com (X. Zhang).
Peer review under responsibility of Institute of Rock and Soil Mechanics, Chinese Academy of Sciences.

https://doi.org/10.1016/j.jrmge.2021.12.005

(Jongmans, 1990; Wu et al., 1998; Nateghi, 2011). Hao et al. (2001) investigated the wave propagation laws in jointed rock mass by blast tests. The influences of rock joints on attenuation characteristics of peak particle velocity (PPV) were discussed. Ye et al. (2008) performed a field explosion experiment on the propagation and attenuation laws of waves in a deep coal mine. It was found that the maximum amplitude of wave is exponentially related to the propagation distance. Lu et al. (2010) studied the propagation laws and frequency spectrum evolution rules of blast-induced shock waves in Sanhejian coal mine. Zhou et al. (2016) conducted field explosion experiments to verify the attenuation of dominant frequency. Roy et al. (2016) studied the attenuation phenomenon of explosion vibrations in an underground metal mine. It was concluded that the PPV of ground motion is inversely proportional to the square root of scale distance (SD). Tian et al. (2019) carried out a series of blasting tests in Dizong tunnel. The spectrum characteristics and frequency-energy change laws of the blasting signals were studied by analyzing the monitoring data. Jayasinghe et al. (2019) experimentally studied the PPV attenuation laws of blast-induced signals along the interface of soil and rock. The effects of the soil-rock interface on stress wave propagation were analyzed. Based on the collected blast-induced signals, various attenuation formulae have been proposed to predict PPV and frequency (Kahriman, 2002, 2004; Ulusay et al., 2004; Kumar et al., 2016). On the other hand, with the rapid development of computer technology, numerical simulation has also become a promising method to understand the attenuation characteristics of stress waves (Wu et al., 2004; Zhu et al., 2007; Ainalis et al., 2017). Chen and Zhao (1998) numerically found that the discontinuities in the rock masses have great effects on the attenuation of blast waves by universal distinct element code (UDEC). Liu et al. (2019) investigated the propagation and attenuation characteristics of shock waves in coal-rock medium at Zhuji coal mine using three-dimensional finite difference code FLAC3D.

As mentioned above, the propagation and attenuation characteristics in different rock media have been investigated by explosion tests in mines and underground caverns. However, the wave components of explosion signals are complex due to the interference of explosive shock. The spectrum ranges of explosion signals are much different from those of MS signals (Ma et al., 2015; Lu et al., 2018; Tian et al., 2019). The spectrum components of MS signals have low-frequency characteristics, generally ranging from 100 Hz to 500 Hz, while the frequency spectrum of blasting signals exceeds 5000 Hz. It is inappropriate to study the energy attenuation laws of MS signals using explosion tests. To investigate the attenuation laws of MS signals, a pendulum impact test facility is designed for exciting seismic signals in this study. The spectrum components of impact-induced seismic waves are relatively similar with those of MS signals. The configuration of this facility is practically operable and convenient than explosion, and it can provide a method for stimulating repeatable seismic waves. Based on the recorded impact-induced signals, the attenuation laws of seismic energy and PPV are studied for deep tunnels.

In this study, using a pendulum impact test facility and MS monitoring system, a series of field attenuation experiments is carried out in a deep tunnel excavated by the tunnel boring machine (TBM). Based on continuous wavelet transform (CWT) and wavelet packet analyses, the time-frequency characteristics and energy distribution laws of impact-induced signals are revealed. The attenuation characteristics of seismic energy and PPV are explored by processing the recorded signals. The relationship between energy attenuation coefficient and wave impedance is established in this scenario. Furthermore, a new method is proposed to calculate the released source energy based on the attenuation characteristics of seismic energy.

2. Engineering background and geological conditions

The headrace tunnel is situated at the Xinjiang Uygur Autonomous Region of China. This tunnel traverses the Tianshan mountains with an excavation length of 41.8 km and diameter of 6.5 m. The axis of this tunnel is about NE12°. Geological profile of this headrace tunnel is shown in Fig. 1. More than 50% of overburden along this tunnel is greater than 1000 m. The maximum buried depth is 2300 m. The tunnel section from chainage K0+000 to K9+800 is excavated by drill-and-blast (DB) method. The remaining tunnel section is excavated by two TBMs from chainage K9+800 to K41+800.

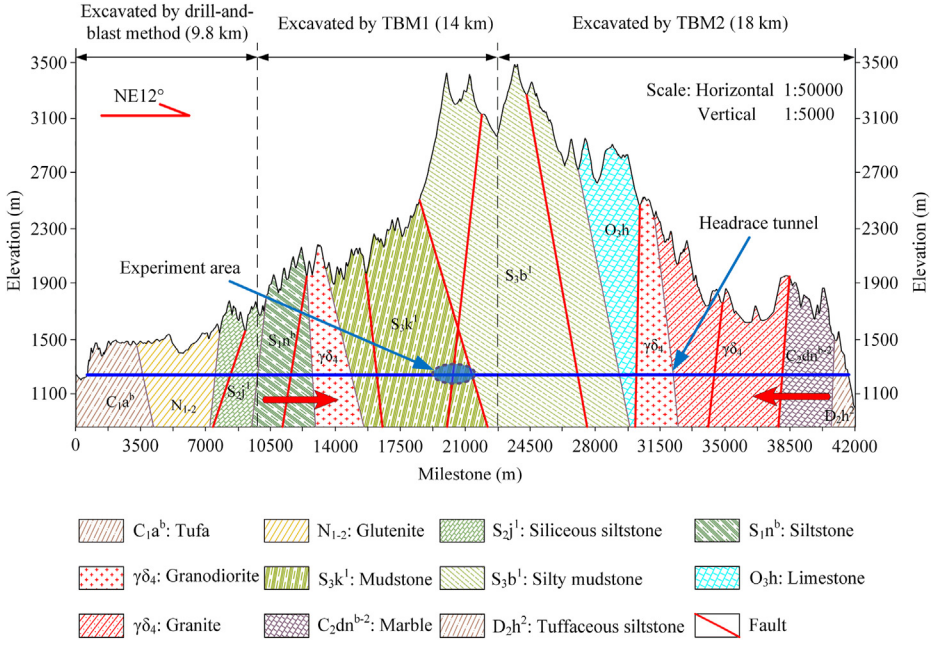

Fig. 1. Geological profile along the headrace tunnel.

The geological structure of this region is composed of the Borokonu complex anticline, which is characterized by Variscan orogeny. The strong squeeze folds, corrugation structures and steeply inclined faults are well developed in this region. As shown in Fig. 1, the steeply inclined faults consist of many groups of faults with NE, NW, NNW and EW directions. The dominant stratum has a strike in EW direction with a steep dip. The lithology formations exposed in this region are composed of siliceous siltstone of Nileke group (S_1n), medium-thick metasiltstone of Jifuke group (S_2j), metamorphic mudstone and fine sandstone of Kuruer group (S_3k), and Variscan granodiorite ($\gamma\delta_4$).

Due to the large depth and strong tectonic movement, high in situ stress is frequently encountered during the excavation of this tunnel. The magnitude of in situ stress was measured by overcoring method at chainage K13+160 (overburden of 740 m) (Sjöberg et al., 2003). It shows that the maximum horizontal principal stress is approximately 33.4 MPa, whose azimuth is parallel to the tunnel axis (NE12°). The intermediate and minimum principal stresses are approximately 25.3 MPa and 22.6 MPa, respectively, whose azimuths are −78.4° and 164.1°, respectively. The maximum depth reaches 2268 m at chainage K24+450. The magnitude of the maximum principal stress is estimated above 50 MPa in the surrounding rock masses. Thus, the stress-induced rock failure will be encountered due to the high in situ stress. In the construction of the tunnel at chainage K9+500–K14+300, a series of mild and moderate rockbursts has occurred at the sidewalls and the crown of the tunnel (Liu et al., 2020).

3. Schemes of attenuation experiments

3.1. Study area

The study area is located at chainage K19+600–K19+628. The buried depth is about 2200 m. The lithology around this area is silty mudstone of Kuruer group (S_3k^1). The density of the surrounding rock masses is 2738 kg/m^3. The uniaxial compressive strength (UCS) of rock around the study area is 48.56 MPa, and its elastic modulus is 13.4 GPa. The geological sketch and experimental layout are shown in Fig. 2. A set of bedding planes is well developed, and filled with thin-layer calcites. Average spacing and trace length of bedding planes are 0.1 m and 20.4 m, respectively. The attitudes of these bedding planes are NW30° ∠ 40° approximately. According to Chinese standard GB50487 (2008), the surrounding rock mass of the study area is categorized as Class III.

3.2. Pendulum impact facility

To excite available seismic sources, a pendulum impact facility is designed for generating repetitive impact-induced signals. The facility mainly consists of steel base, rolling bearing, dial, oscillating bar and pendulums. The size of steel base is 200 mm × 200 mm × 10 mm (length × width × height). The length of oscillating bar is 0.5 m. There are three pendulums with different masses, i.e. 1 kg, 2.5 kg and 5 kg. To avoid the waveform interference caused by fragmented rock masses, a steel cushion block is tightly inserted into the rock masses at the impact point. As shown in Fig. 3, the pendulum impact facility is fixed to right sidewall of this tunnel by expansion bolts. It is available to generate impact-induced vibration signals at different energy levels by controlling the drop height of pendulums.

3.3. Experimental procedure

This pendulum impact test facility provides a method for stimulating seismic waves repeatedly. The pendulum falls freely from different heights at 0.94 m, 0.64 m and 0.22 m, corresponding to the scales of dial at 180°, 130° and 80°, respectively (Fig. 3b). The input impact-energy is equal to the gravitational potential energy of the pendulum. Then, the values of input impact-energy (I_E) range from 2.2 J to 47 J, as listed in Table 1. To obtain reliable impact-

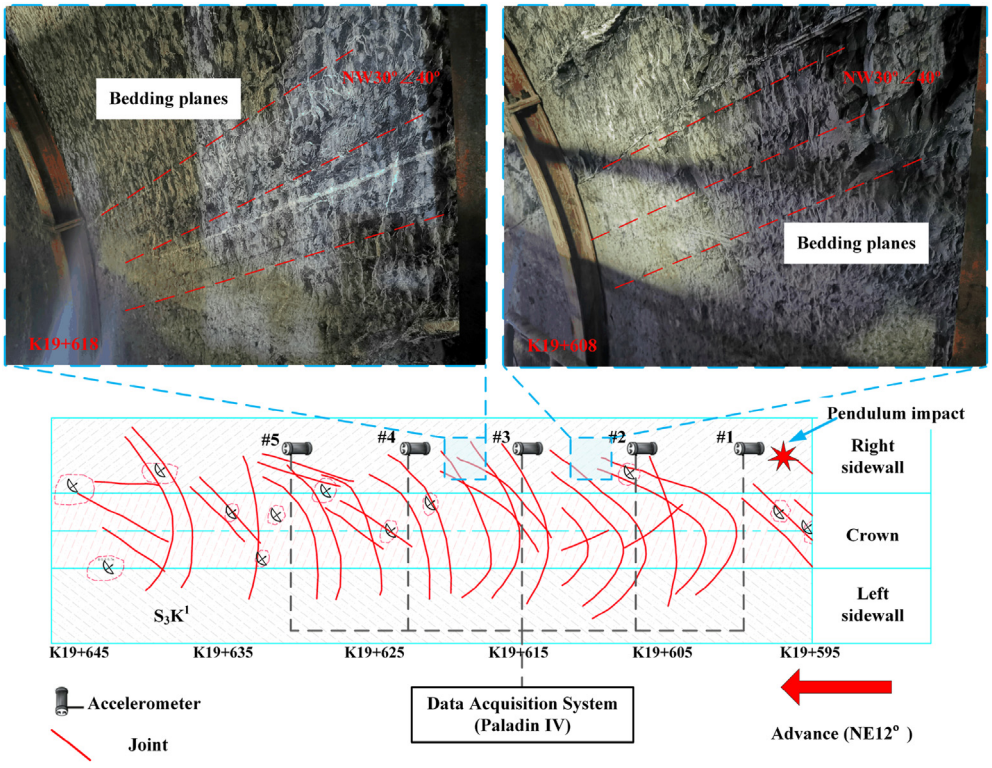

Fig. 2. Geological sketch and experimental layout.

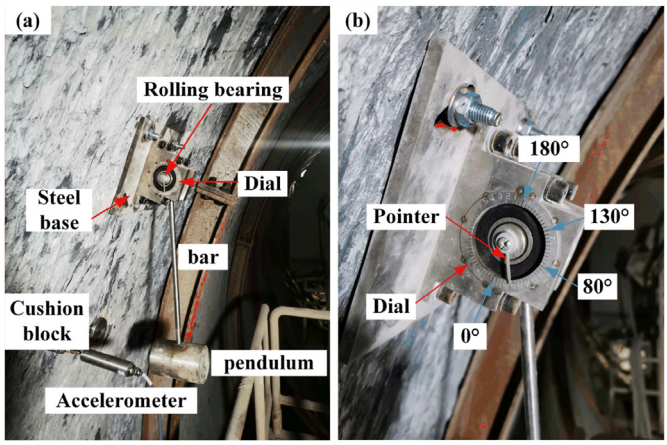

Fig. 3. Installation of pendulum impact facility.

Table 1
Values of input impact-energy (I_E).

Scale of dial (°)	Input impact-energy (J)		
	1 kg pendulum	2.5 kg pendulum	5 kg pendulum
180	9.4	23.5	47
130	6.4	16	32
80	2.2	5.5	11

induced waveforms, six tests are performed for each test scenario. A high-resolution MS monitoring system, manufactured by Engineering Seismology Group (ESG), is used to record the impact-induced waves in this study (Fig. 4a). The MS monitoring system consists of digital signal processing system and digital signal acquisition system, possessing a 32-bit delta-sigma digital-to-analogue converter (DAC) and a sampling frequency of 10 kHz, respectively. When the recorded signals exceed a given threshold, the MS monitoring system can perform preliminary event detection, using the short time average versus long time average (STA/LTA) algorithm. Besides, to ensure the reliability of signal transmission between the signal acquisition system and accelerometers, twisted pair cables and fiber optics are used to connect these system devices. The uniaxial accelerometers have a frequency response range of 50–5000 Hz and a sensitivity of 30 V/g. As shown in Fig. 2, the sensor array is distributed in a straight line along the axis of the tunnel, and the intervals of accelerometers are 6.7 m, 7.4 m, 6.8 m and 5.6 m from sensors #1 to #5. To install the sensors on the sidewall tightly, five boreholes, with a depth of 200 mm and diameter of 10 mm, are drilled by electric hand-drill. The uniaxial accelerometers are mounted in the boreholes by anchor resin. Then, the impact-induced waves can be received by accelerometers #1–#5 in sequence.

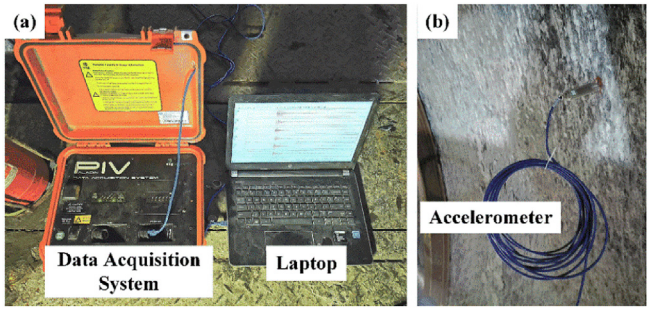

Fig. 4. (a) Data acquisition system, and (b) Installation of accelerometer.

4. Experimental results

4.1. Seismic energy attenuation characteristics

Due to the viscoelastic and anisotropic properties, the attenuation of energy will occur when the seismic waves propagate through rock medium. There are three energy attenuation modes, i.e. geometrical spreading, intrinsic absorption and scattering attenuation (Gibowicz and Kijko, 1994; Fu et al., 2018; Barbosa et al., 2019). In seismology, a dimensionless quality factor (Q) is used to describe the energy attenuation of seismic waves (Johnston, 1979; Wanniarachchi et al., 2017), which is defined as a fractional energy loss per cycle:

$$Q = -\frac{2\pi E}{\Delta E} \tag{1}$$

where E is the total energy and ΔE is the energy loss per cycle (T). Eq. (1) can be rewritten as follows:

$$Q = -\frac{2\pi E}{T\frac{dE}{dt}} \tag{2}$$

$$\frac{dE}{E} = -\frac{2\pi}{TQ}dt \tag{3}$$

where t is the time. Then, the energy attenuation of seismic waves can be expressed in exponential function form as follows:

$$E = E_0 e^{-\frac{2\pi t}{TQ}} = E_0 e^{-\frac{2\pi f}{Qv}x} = E_0 e^{-\alpha_E x} \tag{4}$$

where E_0 is the MS energy at the source; f is the frequency; v is the wave velocity; x is the propagation distance; and the term $2\pi f/(Qv)$ is defined as the energy attenuation coefficient α_E (m^{-1}), which can be used as an index of energy attenuation. As the value of attenuation coefficient α_E decreases, the energy loss also decreases.

4.2. Analysis of the impact-induced signals

The impact-induced signals at different monitoring points (#1–#5) are recorded by MS monitoring system. Acceleration-time curves are measured for each impact test. Then, the velocity-time curves can be obtained by numerically integrating the acceleration-time curves. For instance, when the value of input impact-energy is 47 J, Fig. 5 shows the measured acceleration-time curves at sensors #1–#5, and the corresponding velocity-time curves are presented in Fig. 6. By picking the first arrivals of seismic waveforms in Fig. 5, the velocity information of the test area can be measured. The distance and difference of arrival times between sensors #1 and #5 are 26.5 m and 7.26 ms, respectively. The average P-wave velocity can be calculated as 3650 m/s. Besides, to present the spectrum characteristics intuitively, the two-dimensional spectra for waveforms #1–#5 are obtained by the fast Fourier transform (FFT), as shown in Fig. 7. It can be seen that the dominant frequency of waveforms is gradually decreased as the propagation distance increases. Moreover, CWT and wavelet packet transform are used to analyze the time-frequency characteristics and the energy distribution of these signals, respectively.

4.2.1. CWT analysis

CWT provides a multi-scale time-frequency analysis for non-stationary signals, which has been widely used in seismology (Mallet, 1999; Kaveh, 2019). CWT is defined as the inner product of a dilated and translated wavelet with the original signal (Mallet, 1999). By translation and scaling of the wavelet function with a variable-size window, the similarity coefficients can be obtained

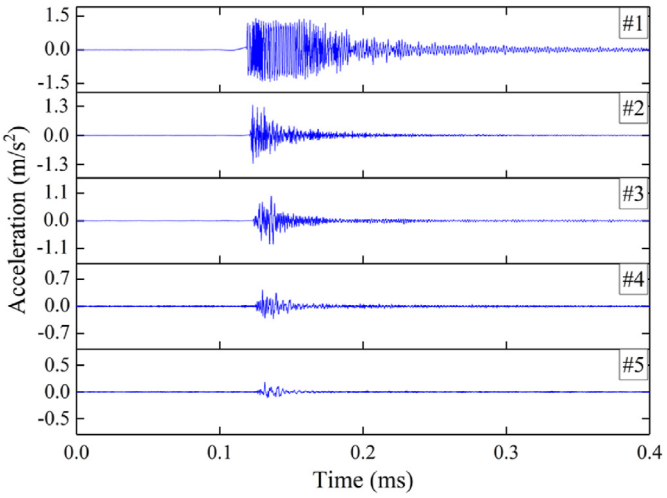

Fig. 5. Acceleration-time curves of sensors #1–#5.

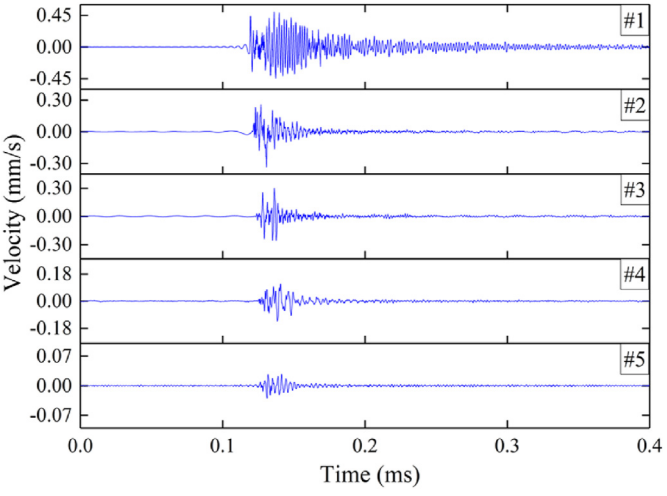

Fig. 6. Velocity-time curves of sensors #1–#5.

throughout the signal (Whitney, 2019). Therefore, CWT can present the local information of signals in time-frequency domain with high resolution. In this study, CWT is introduced to analyzing the time-frequency characteristics of impact-induced signals.

As shown in Fig. 6, the velocity waveforms at monitoring points #1–#5 are attenuated successively. By programming about CWT in MATLAB software, the wavelet spectra of these velocity waveforms are shown in Fig. 8. It can be seen that the dominant frequency of sensors #1–#5 are 612 Hz, 371 Hz, 362 Hz, 332 Hz and 214 Hz, respectively. The dominant frequency of signals gradually decreases with the increase of propagation distance. As shown in Fig. 8a and b, there are high-frequency components between 1000 Hz and 2500 Hz. However, these high-frequency components are attenuated significantly in Fig. 8e. The frequency spectra of velocity waveforms display low-frequency characteristics as the propagation distance increases. It seems that the bedding planes may have high-frequency filter effects on seismic waves.

4.2.2. Wavelet packet transform analysis

The wavelet packet transform is a signal processing technique to decompose the different frequency components of the signals (Tian et al., 2019). By using the wavelet packet energy analysis program in MATLAB software, the energy distribution characteristics of different frequency bands can be analyzed. The selection of wavelet functions depends on the shape of the input signals. Due to the good compact support, smoothness and symmetry of Daubechies wavelet system (Daubechies, 1990; Huang et al., 2019), db8 wavelet function is selected to analyze the impact-induced signals in Fig. 6. These signals are decomposed into 8 layers with 2^8 (256) frequency bands. The width of each frequency band is 19.53 Hz. As shown in Fig. 8, the dominant frequency components of the signal #1 are distributed below 1000 Hz. Then, the 1st–51st frequency bands (0–996.03 Hz) are selected to analyze the energy distribution characteristics of these signals. The percentages of energy distribution with different frequency bands are presented in Fig. 9.

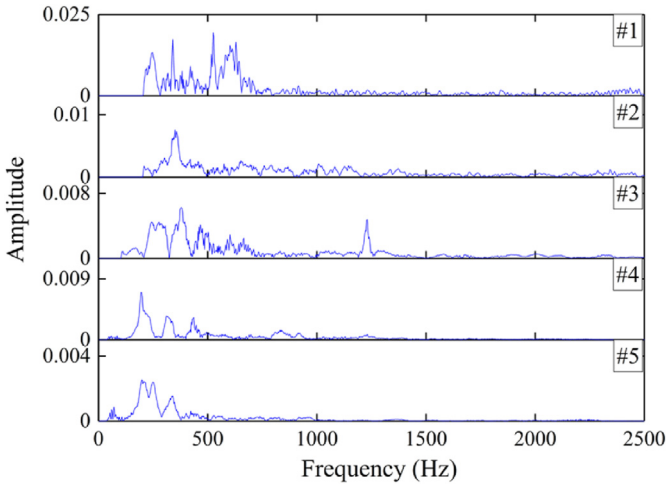

Fig. 7. Frequency-domain curves of sensors #1–#5 by FFT.

For the signal received by sensor #1, the wave energy is mainly distributed in two frequency bands of 200–300 Hz and 500–700 Hz, accounting for 28.07% and 47.47%, respectively. As the impact-induced signal propagates from sensors #1 to #5, the percentage of energy distribution in the frequency bands of 500–700 Hz significantly declines from 47.47% to 1.56%. However, the percentage of energy distribution in the frequency bands of 200–300 Hz increases gradually from 28.07% to 59.46%. Due to the reflection and scattering effects on the propagation path, the distribution of energy is gradually concentrated in the low-frequency bands of 200–300 Hz.

4.3. Energy and PPV attenuation laws in deep tunnels

To understand the energy attenuation laws of seismic waves in deep tunnels, the impact-induced signals at different monitoring points (#1–#5) are recorded by MS monitoring system. The energy value of impact-induced wave can be calculated as (Martinez-Martinez et al., 2011):

$$E_T = \frac{1}{2}\Delta m \int_{t_s}^{t_e} v^2(t)\mathrm{d}t \tag{5}$$

where E_T represents the total energy of impact-induced signal; Δm is the unit mass; t_s and t_e are the start and end times of the calculation period, respectively; and $v(t)$ is the velocity function.

When the value of input impact-energy is 47 J, the corresponding velocity-time curves of sensors #1–#5 are presented in Fig. 6. The energy values at different monitoring points (#1–#5) can be calculated as 3.051 J, 0.489 J, 0.539 J, 0.164 J and 0.048 J,

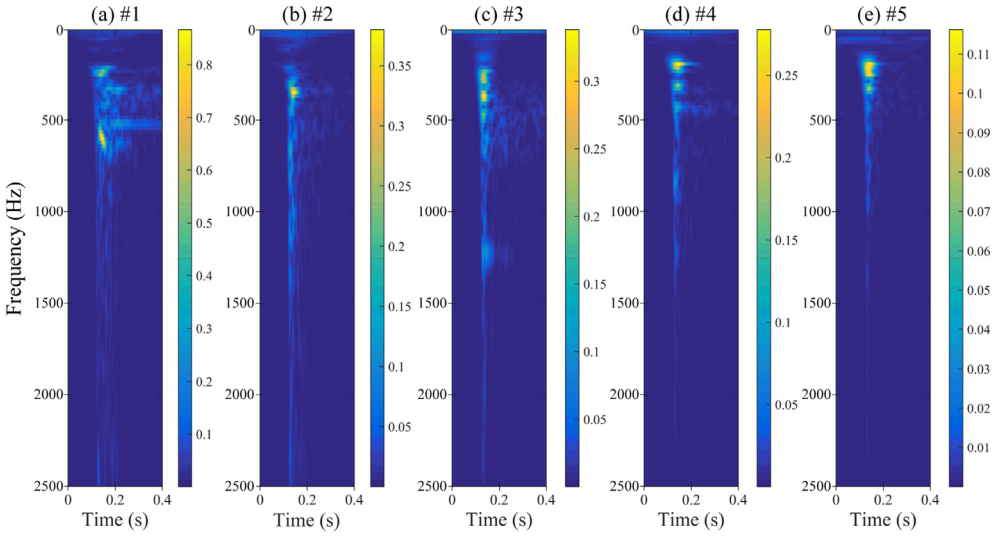

Fig. 8. Wavelet spectra of sensors (a) #1, (b) #2, (c) #3, (d) #4, and (e) #5.

respectively. As shown in Fig. 10, the intensity of impact-induced signal decreases greatly as the propagation distance increases. The energy attenuation laws can be exponentially fitted by Eq. (6) with coefficient of determination R^2 of 0.948. In addition, the PPV is defined as the maximum amplitude of the vibration velocity. According to Fig. 6, the PPV values at different monitoring points (#1–#5) are 0.457 m/s, 0.337 m/s, 0.285 m/s, 0.093 m/s and 0.05 m/s, respectively. The PPV attenuation laws can be exponentially fitted by Eq. (7) with R^2 of 0.928.

$$E_T = 3.29e^{-0.23x} \tag{6}$$

$$PPV = 0.49e^{-0.05x} \tag{7}$$

Due to the presence of geological discontinuities, attenuation effects of seismic waves have been investigated in different scenarios (Wu et al., 1998; Lu et al., 2010; Jayasinghe et al., 2019). The energy attenuation of seismic waves is closely associated to the physical properties and structural features of rock medium. In this study, the rock mass contains a set of bedding planes filled with thin-layer calcites. The angle between the bedding planes and measurement alignment is 40°. When the seismic waves propagate obliquely through the bedding rock masses, the wave reflection and refraction would occur between the layers. It may have a great contribution on the energy attenuation of seismic waves.

Under the conditions of different input impact-energy, i.e. 2.2 J, 5.5 J, 6.4 J, 9.4 J, 11 J, 16 J, 23.5 J and 32 J, the calculated energy and PPV values at different monitoring points are used to study the attenuation laws in deep tunnels. The scatter diagrams of energy and PPV related to propagation distance are presented in Fig. 11. It can be seen that the attenuation degree of energy is larger than that of PPV, and the near-field attenuation of energy is much greater than that of the far-field.

By fitting the attenuation data at different input impact-energy levels, the attenuation laws of energy and PPV are shown in Fig. 12. The energy and PPV attenuation of impact-induced waves are exponentially related to the propagation distance. The energy values of signals decrease by 85% within the propagation distance of 10 m, while the attenuation degree of PPV is relatively small. The attenuation coefficients of energy (α_E) and PPV (α_P) are tabulated in Table 2. The attenuation coefficients of energy are much larger than

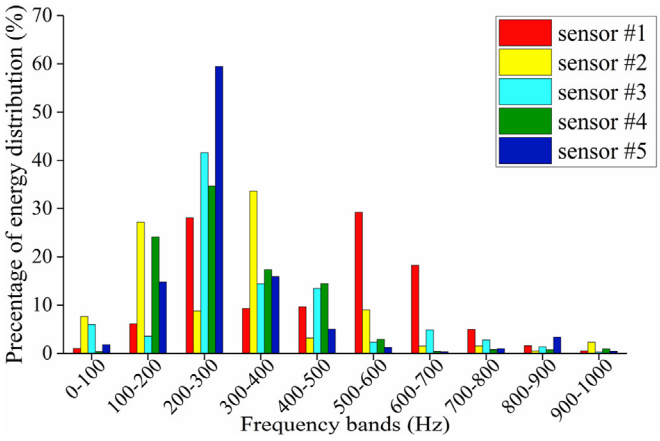

Fig. 9. Percentages of energy distribution in different frequency bands (sensors #1–#5).

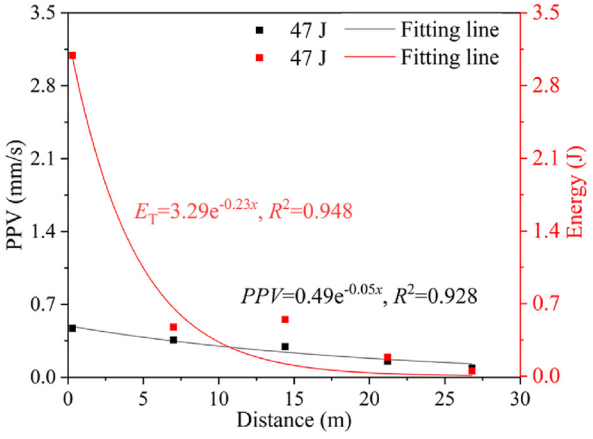

Fig. 10. Attenuation laws of energy and PPV at input impact-energy of 47 J.

those of PPV. The values of α_E/α_P range from 3.216 to 4.731. It means that the attenuation of energy is more sensitive than that of PPV.

The relationship between the energy attenuation coefficient and input impact-energy is shown in Fig. 13, which can be fitted by Eq. (8) with R^2 of 0.855.

$$\alpha_E = 0.54 I_E^{-0.221} \tag{8}$$

With the increase of input impact-energy (I_E) from 2.2 J to 47 J, the energy attenuation (α_E) coefficient gradually decreases from 0.447 m^{-1} to 0.23 m^{-1} in a form of power function. The relationship between the energy attenuation coefficient and impact-energy of waves is in agreement with B. Li et al. (2020). The energy attenuation coefficient decreases significantly at the beginning. When the input impact-energy exceeds 20 J, the slope of this curve gradually becomes stable. It can be inferred that the higher impact-energy of the induced waves may enhance the normal stiffness of joints to facilitate the transmission of waves. The energy attenuation coefficient will be changed with the intensity of MS events. In this scenario, the energy attenuation coefficient of high-energy MS events will be smaller than that of low-energy MS events.

4.4. Relationship between energy attenuation coefficient and wave impedance

In the micro-perspective of rock medium, the most important factors causing the energy attenuation of seismic waves are the compactness of mineral particles and the fissure planes inside the rock. As the compactness of mineral particles increases, the porosity becomes lower, and thus the energy attenuation of seismic waves would decrease. On the other hand, with the density of fissure planes increases, the reflection and scattering of waves occur frequently, and the energy attenuation of seismic waves would increase. The wave impedance reflects the reflection and transmission ability of stress wave in the rock medium, and its value is equal to the product of the rock density and P-wave velocity (Tian et al., 2019). The density of the rock can reflect the compactness between the internal particles, and the P-wave velocity can reflect the integrity of the rock. Due to the difference of the wave impedance characteristics in rock masses, the seismic waves would generate reflection and transmission. The portion of seismic energy will be scattered. Therefore, the propagation and attenuation characteristics of seismic waves are closely associated with the wave impedance characteristics of the rock medium.

To explore the relationship between energy attenuation coefficient and wave impedance, 10 pendulum impact tests at different tunnel sections are conducted. The corresponding rock density and P-wave velocity can be measured at each testing scenario. Therefore, the values of P-wave velocity, rock density, wave impedance and energy attenuation coefficient are listed in Table 3. Note that the attenuation coefficients of energy are calculated at the same impact-energy level (2.2 J).

According to the data in Table 3, the relationship between energy attenuation coefficient and wave impedance can be drawn in Fig. 14, which is fitted by Eq. (9) with R^2 of 0.81.

$$\alpha_E = -0.046Z + 0.898 \tag{9}$$

where Z denotes the wave impedance. It can be seen that the energy attenuation coefficient has a negative correlation with wave impedance. As the value of wave impedance increases, the energy attenuation coefficient decreases. It means that the energy loss of seismic waves decreases with less reflection and scattering. Then, an empirical relationship between energy attenuation coefficient and wave impedance is established in Eq. (9). It provides a method to estimate the energy attenuation coefficient in this scenario.

5. Determination of the released source energy

The source energy of MS events is usually used as a quantitative evaluation index for the rockburst intensity classification (Chen et al., 2015; Liu et al., 2020). Therefore, the reliable estimation of source energy is important for rockburst classification and forecasting. The relationship between the seismic energy at the source and residual energy at a specific location is formulated in Eq. (4). The Napierian logarithmic transformation of Eq. (4) is expressed as follow:

$$\ln E = -\alpha_E x + \ln E_0 \tag{10}$$

where E is the residual energy of the monitored seismic waves, and E_0 is the seismic energy at the source. It is noted that the MS energy (E_0) at the source accounts for 0.1% of the total released source energy (E_R) in the process of rock fracture (McGarr, 1976; Cai et al., 1998).

To determine the seismic energy at the source, three important parameters should be obtained, i.e. the propagation distance, residual energy and energy attenuation coefficient. Based on the simplex location algorithm, coordinates of MS events are measured in the ESG system, and propagation distance between the MS source and the sensor can be calculated. Meanwhile, residual energy of the recorded seismic waves is calculated by Eq. (5). According to the energy attenuation laws described in Section 4.3, the energy attenuation of low-energy MS events is more significant than that of high-energy MS events. The energy attenuation coefficients of seismic waves can be obtained by Eq. (8) in this scenario. However, note that Eq. (8) reveals the relationship between

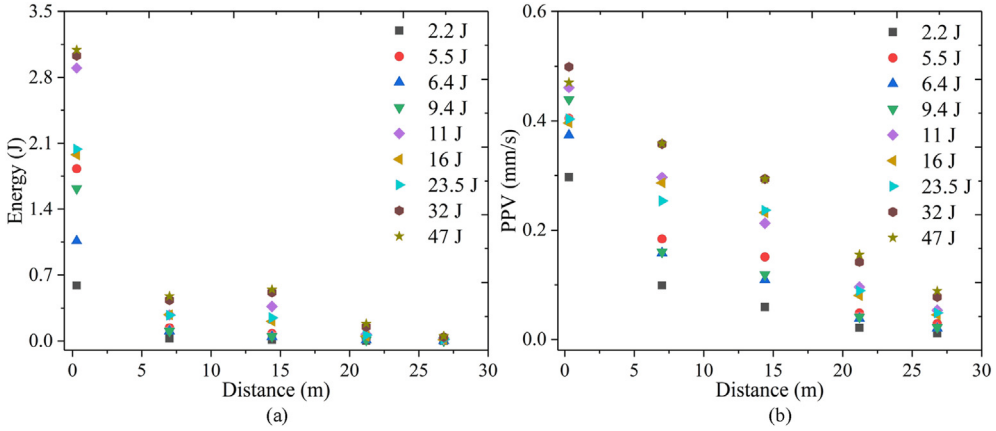

Fig. 11. Scatter diagrams of (a) signal energy and (b) PPV related to propagation distance.

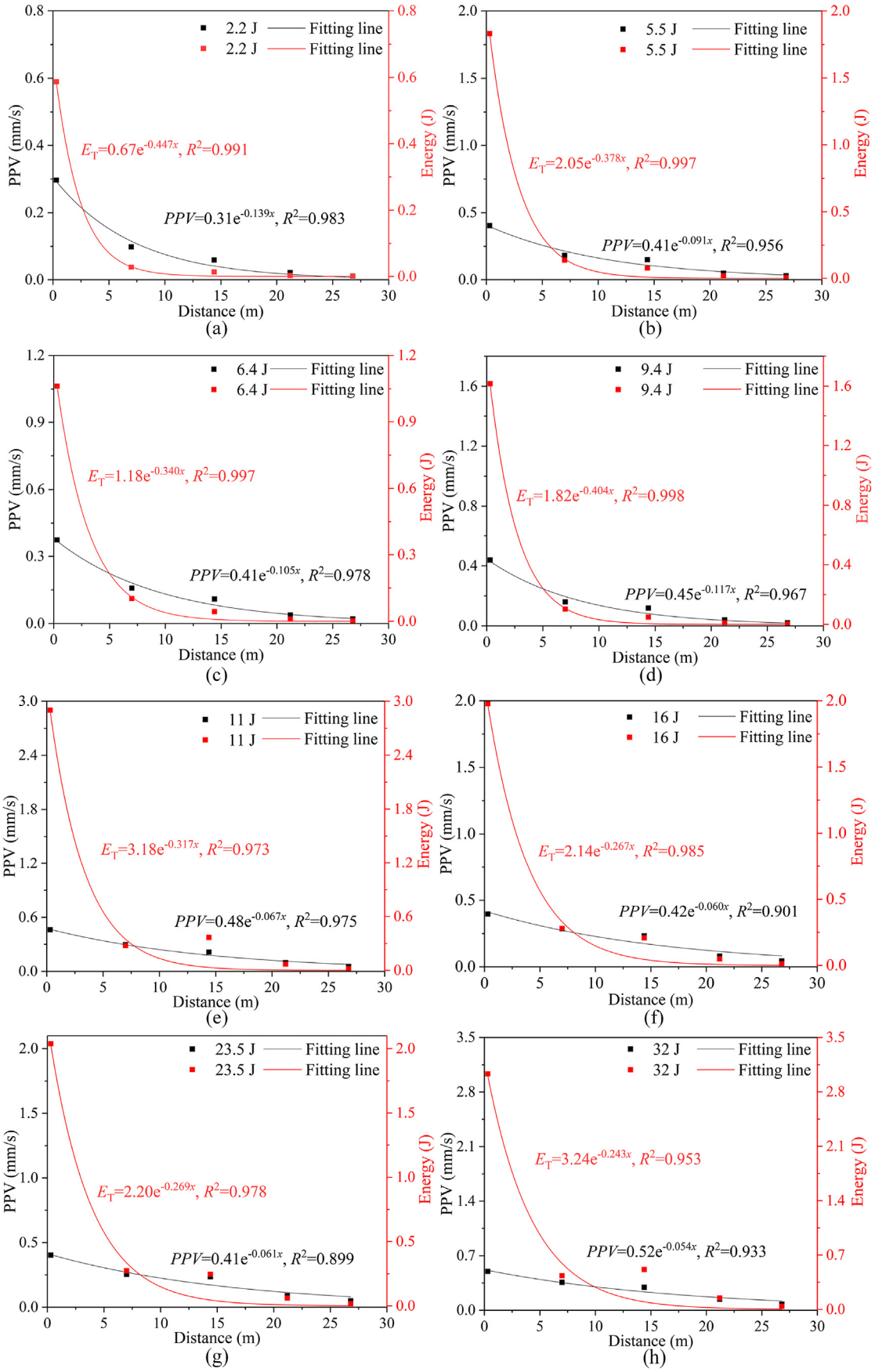

Fig. 12. Attenuation laws of energy and PPV at different input impact-energy levels: (a) 2.2 J, (b) 5.5 J, (c) 6.4 J, (d) 9.4 J, (e) 11 J, (f) 16 J, (g) 23.5 J, and (h) 32 J.

Table 2
Attenuation coefficients of energy and PPV.

Input impact-energy (J)	α_E	α_P	α_E/α_P
2.2	0.447	0.139	3.216
5.5	0.376	0.091	4.132
6.4	0.34	0.105	3.238
9.4	0.404	0.117	3.453
11	0.317	0.067	4.731
16	0.267	0.06	4.45
23.5	0.269	0.061	4.41
32	0.243	0.054	4.5
47	0.23	0.05	4.6

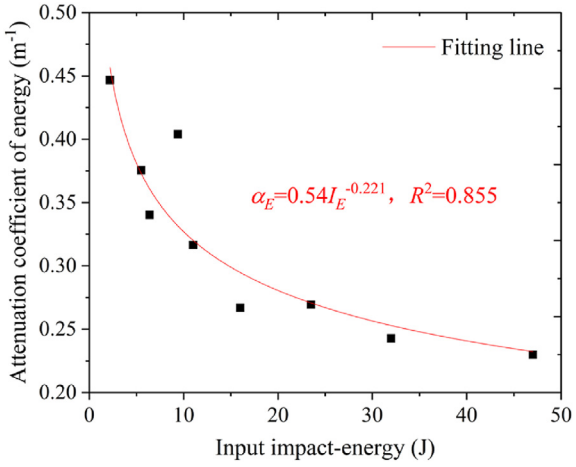

Fig. 13. Relationship between energy attenuation coefficient and input impact-energy.

Table 3
Detailed information of 10 pendulum impact tests.

Date (YY/MM/DD)	Chainage (m)	P-wave velocity (m/s)	Rock density (g/cm^3)	Wave impedance (10^9 g/(m^2 s))	α_E (m^{-1})
2019/10/28	19,331 −19,358	4858.01	2.82	13.70028	0.306
2019/11/9	19,600 −19,628	3647.69	2.738	9.98782	0.446
2019/11/12	19,674 −19,701	5014.5	2.827	14.17652	0.174
2019/11/14	19,714 −19,738	3990.57	2.699	10.77096	0.381
2019/11/17	19,781 −19,809	5126.76	2.72	13.94614	0.323
2019/11/19	19,825 −19,850	5179.69	2.743	14.20865	0.27
2019/11/22	19,913 −19,939	5377.47	2.652	14.26198	0.185
2019/11/29	20,095 −20,123	4858.01	2.82	13.70028	0.306
2019/12/5	20,202 −20,229	5160.41	2.857	14.74403	0.252
2019/12/12	20,353 −20,383	5619.11	2.745	15.42686	0.174

the energy attenuation coefficients and the input impact-energy. Only part of the input impact-energy generated by the pendulum can be converted into seismic wave energy. The conversion efficiency (η_1) is defined as the ratio of the seismic energy at the source (E_0) to the input impact-energy (I_E), which is taken as 20% (Wang et al., 2019). Thus, Eq. (8) can be rewritten as follows:

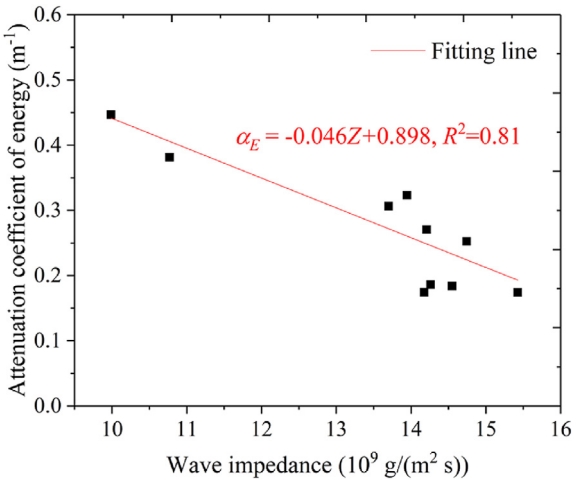

Fig. 14. Relationship between energy attenuation coefficient and wave impedance.

Table 4
Comparison of the released source energy calculated by two methods.

No.	Propagation distance (m)	Released source energy (J)		$E_{R\text{-}N}/E_{R\text{-}S}$
		$E_{R\text{-}N}$ (new method)	$E_{R\text{-}S}$ (ESG system)	
1	110.19	6.52×10^5	6.29×10^5	1.04
2	114.4	4.34×10^5	7.1×10^4	6.11
3	111.26	4.29×10^5	6.1×10^4	7.03
4	112.03	3.52×10^5	5.73×10^4	6.14
5	118.52	4.97×10^5	4.72×10^4	10.53
6	117.13	5.05×10^5	4.41×10^4	11.45
7	109.92	3.09×10^5	2.02×10^4	15.3
8	108.12	3.24×10^5	1.65×10^4	19.64
9	101.83	2.72×10^5	1.49×10^4	18.26
10	108.33	2.55×10^5	3.33×10^3	76.58
11	109.65	2.44×10^5	$1.8 \times \times 10^3$	135.56

$$\alpha_E = 0.54\left(\frac{E_0}{\eta_1}\right)^{-0.221} \tag{11}$$

Combining with Eqs. (10) and (11), the expression of the seismic energy at the source (E_0) is given as Eq. (12), which can be solved by Newton iteration method. Then, a new method is proposed to determine the released source energy.

$$\ln E = -0.54\left(\frac{E_0}{\eta_1}\right)^{-0.221} x + \ln E_0 \tag{12}$$

The values of the released source energy obtained by the ESG system and the new proposed method are compared in Table 4. Eleven MS events recorded by the same monitoring arrays are selected as data samples. The typical MS waveforms are shown in Fig. 15. By processing the MS events in the ESG system, the source coordinates and released source energy ($E_{R\text{-}E}$) can be calculated. The related source parameters are listed in Table 4. In the ESG system, the value of attenuation correction coefficient is generally constant for all recorded MS events (Wandycz et al., 2019; Liu et al., 2020). The estimation of attenuation coefficient depends on the engineering experiences, rather than field investigation. The correction errors would occur in the calculation of source energy. Therefore, to estimate the seismic energy of MS events accurately, the value of attenuation correction coefficient should be adjusted for MS events with different energies, especially for low-energy MS events. In the new proposed method, this energy-dependent

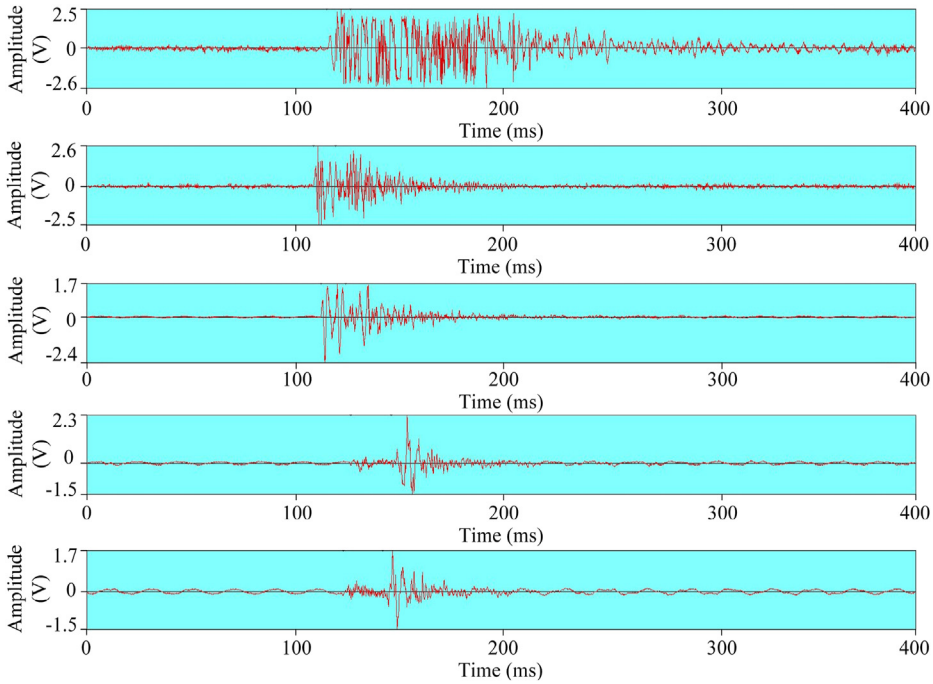

Fig. 15. Typical MS waveforms recorded by the ESG system.

attenuation difference has been properly accounted. Based on the energy attenuation characteristics, the proposed method has a relatively significant attenuation correction for low-energy MS events. As shown in Table 4, it can be seen that there are significant differences between the source energies calculated by two methods ($E_{R\text{-}N}$ and $E_{R\text{-}E}$). The magnitudes of $E_{R\text{-}N}$ are generally larger than those of $E_{R\text{-}E}$. The difference between the $E_{R\text{-}N}$ and $E_{R\text{-}E}$ increases as the decrease of released energy. The ratio of the $E_{R\text{-}N}$ to $E_{R\text{-}E}$ ranges from 1.04 to 135.56.

6. Conclusions

By using a pendulum impact test facility and MS monitoring system, an in situ investigation is carried out to study attenuation laws of MS signals at a deep tunnel. The angle between the bedding planes and measurement alignment is about 40° in this scenario. The in situ stress has a significant influence on the attenuation characteristics. The initial pores in rock masses will be closed under high in situ stress. On the other hand, the in situ stress also has a considerable impact on the deformation and strength characteristics of joints. The stiffness of joints will be enhanced under stresses, which makes it easier for seismic waves to propagate across the joints.

The attenuation laws of seismic energy and PPV are revealed in this study. CWT and wavelet packet analyses are applied to analyzing the attenuation characteristics of impact-induced signals in time-frequency domain. The main conclusions are drawn as follows:

(1) As the impact-induced signal propagates from sensors #1 to #5, the dominant frequency of signals decreases gradually from 612 Hz to 214 Hz. The high-frequency components between 1000 Hz and 2500 Hz attenuate significantly. With the increase in propagation distance, the energy distribution of impact-induced signals is gradually concentrated in the low-frequency bands (200–300 Hz).

(2) According to the measured energy and PPV values at different monitoring points (#1–#5), the energy and PPV attenuation of impact-induced signals are exponentially related to the propagation distance. The attenuation of energy is more sensitive than that of PPV.

(3) As the input impact-energy increases, the energy attenuation coefficient gradually decreases in a form of power function. It can be inferred that the attenuation degree of seismic energy will be changed with the intensity of signals. The energy attenuation degree of low-energy MS events is more significant than that of high-energy MS events.

(4) The relationship between energy attenuation coefficient and wave impedance is revealed based on 10 pendulum impact tests. An empirical equation between energy attenuation coefficient and wave impedance is established in this scenario. The energy attenuation coefficient has a negative correlation with wave impedance of the rock masses.

(5) Based on the energy attenuation characteristics for MS events with different energies, an equation is proposed to calculate the released source energy in the deep tunnel. It provides a more reasonable source energy index for rockburst risk and disaster assessment.

Declaration of competing interest

The authors declare that they have no known competing financial interests or personal relationships that could have appeared to influence the work reported in this paper.

Acknowledgments

The support provided by the National Natural Science Foundation of China (Grant Nos. 51978541, 41941018 and 51839009) is gratefully acknowledged.

References

Ainalis, D., Kaufmann, O., Tshibangu, J.P., Verlinden, O., Kouroussis, G., 2017. Modelling the source of blasting for the numerical simulation of blast-induced ground vibrations: a review. Rock Mech. Rock Eng. 50 (1), 171–193.

Barbosa, N.D., Caspari, E., Rubino, J.G., Greenwood, A., Baron, L., Holliger, K., 2019. Estimation of fracture compliance from attenuation and velocity analysis of full-waveform sonic log data. J. Geophys. Res. Solid Earth 124, 2738–2761.

Cai, M., Kaiser, P.K., Martin, C.D., 1998. A tensile model for the interpretation of microseismic events near underground openings. Pure Appl. Geophys. 153 (1), 67–92.

Cai, M., Kaiser, P.K., Martin, C.D., 2001. Quantification of rock mass damage in underground excavations from microseismic event monitoring. Int. J. Rock Mech. Min. Sci. 38 (8), 1135–1145.

Chen, S.G., Zhao, J., 1998. A study of UDEC modelling for blast wave propagation in jointed rock masses. Int. J. Rock Mech. Min. Sci. 35 (1), 93–99.

Chen, B.R., Feng, X.T., Li, Q.P., Luo, R.Z., Li, S.J., 2015. Rock burst intensity classification based on the radiated energy with damage intensity at Jinping II hydropower station, China. Rock Mech. Rock Eng. 48 (1), 289–303.

Dai, F., Li, B., Xu, N.W., Fan, Y.L., Zhang, C.Q., 2016. Deformation forecasting and stability analysis of large-scale underground powerhouse caverns from microseismic monitoring. Int. J. Rock Mech. Min. Sci. 86, 269–281.

Daubechies, I., 1990. The wavelet transform time-frequency localization and signal analysis. IEEE Trans. Inf. Theor. 36 (5), 961–1005.

Feng, X.T., Chen, B.R., Li, S.J., Zhang, C.Q., Xiao, Y.X., Feng, G.L., Zhou, H., Qiu, S.L., Zhao, Z.N., Yu, Y., Chen, D.F., Ming, H.J., 2012. Studies on the evolution process of rockbursts in deep tunnels. J. Rock Mech. Geotech. Eng. 4 (4), 289–295.

Fu, B.Y., Guo, J., Fu, L.Y., Glubokovskikh, S., Galvin, R.J., Gurevich, B., 2018. Seismic dispersion and attenuation in saturated porous rock with aligned slit cracks. J. Geophys. Res. Solid Earth 123, 6890–6910.

GB50487, 2008. Code for Engineering Geological Investigation of Water Resources and Hydropower. China Planning Press, Beijing, China.

Gibowicz, S.J., Kijko, A., 1994. An Introduction to Mining Seismology. Polish Academy of Sciences, Warsaw, Poland.

Glazer, S.N., 2016. Mine Seismology: Data Analysis and Interpretation. Springer International Publishing, Switzerland.

Hao, H., Wu, Y.K., Ma, G.W., Zhou, Y.X., 2001. Characteristics of surface ground motions induced by blasts in jointed rock mass. Soil Dynam. Earthq. Eng. 21 (2), 85–98.

Huang, D., Cui, S., Li, X.Q., 2019. Wavelet packet analysis of blasting vibration signal of mountain tunnel. Soil Dynam. Earthq. Eng. 117, 72–80.

Jayasinghe, B., Zhao, Z.Y., Chee, A.G.T., Zhou, H.Y., Gui, Y.L., 2019. Attenuation of rock blasting induced ground vibration in rock-soil interface. J. Rock Mech. Geotech. Eng. 11 (4), 770–778.

Johnston, D.H., Toksöz, M.N., Timur, A., 1979. Attenuation of seismic waves in dry and saturated rocks: II. Mechanisms. Geophysics 44 (4), 691–711.

Jongmans, D., 1990. In situ measurement in soils. Eng. Geol. 29, 99–118.

Kahriman, A., 2002. Analysis of ground vibrations caused by bench blasting at Can Openpit Lignite Mine in Turkey. Environ. Geol. 41 (6), 653–661.

Kahriman, A., 2004. Analysis of parameters of ground vibration produced from bench blasting at a limestone quarry. Soil Dynam. Earthq. Eng. 24 (11), 887–892.

Kaveh, M.S., Mansouri, R., Keshavarz, A., 2019. Automatic P-wave picking using undecimated wavelet transform. J. Seismol. 23 (5), 1031–1046.

Kumar, R., Choudhury, D., Bhargava, K., 2016. Determination of blast-induced ground vibration equations for rocks using mechanical and geological properties. J. Rock Mech. Geotech. Eng. 8 (3), 341–349.

Li, S.J., Feng, X.T., Li, Z., Chen, B., Zhang, C., Zhou, H., 2012. In situ monitoring of rockburst nucleation and evolution in the deeply buried tunnels of Jinping II hydropower station. Eng. Geol. 137, 85–96.

Li, Z.L., Li, J.C., Li, H.B., Zhao, J., 2020. Effects of a set of parallel joints with unequal close-open behavior on stress wave energy attenuation. Waves Random Complex Media 2, 1–25.

Li, B., Ding, Q.F., Xu, N.W., Lei, Y.F., Xu, Y., Zhu, Z.P., Liu, J.F., 2020. Mechanical response and stability analysis of rock mass in high geostress underground powerhouse caverns subjected to excavation. J. Cent. South Univ. 27, 2971–2984.

Li, X., Mao, H.Y., Li, B., Xu, N.W., 2021. Dynamic early warning of rockburst using microseismic multi-parameters based on Bayesian network. Eng. Sci. Technol. 24 (3), 715–727.

Liang, Z.Z., Xue, R.X., Xu, N.W., Li, W.R., 2020. Characterizing rockbursts and analysis on frequency-spectrum evolutionary law of rockburst precursor based on microseismic monitoring. Tunn. Undergr. Space Technol. 105, 103564.

Liu, G.J., Karakus, M., Mu, Z.L., 2019. Propagation and attenuation characteristics of rockburst-induced shock waves in coal-rock medium. Arabian J. Geosci. 12 (4), 113.

Liu, Q.S., Wu, J., Zhang, X.P., Tang, L.X., Bi, C., Li, W.W., Xu, J.L., 2020. Microseismic monitoring to characterize structure-type rockbursts: a case study of a TBM-excavated tunnel. Rock Mech. Rock Eng. 53, 2995–3013.

Lu, C.P., Dou, L.M., Wu, X.R., Xie, Y.S., 2010. Case study of blast-induced shock wave propagation in coal and rock. Int. J. Rock Mech. Min. Sci. 47 (6), 1046–1054.

Lu, C.P., Liu, Y., Zhang, N., Zhao, T.B., Wang, H.Y., 2018. In-situ and experimental investigations of rockburst precursor and prevention induced by fault slip. Int. J. Rock Mech. Min. Sci. 108, 86–95.

Ma, T.H., Tang, C.A., Tang, L.X., Zhuang, D.Y., Wang, L., 2015. Rockburst characteristics and microseismic monitoring of deep-buried tunnels for Jinping II hydropower station. Tunn. Undergr. Space Technol. 49, 345–368.

Mallet, S., 1999. A Wavelet Tour of Signal Processing, second ed. Academic Press, Waltham, USA.

Martinez-Martinez, J., Benavente, D., Garcia-del-Cura, M.A., 2011. Spatial attenuation: the most sensitive ultrasonic parameter for detecting petrographic features and decay processes in carbonate rocks. Eng. Geol. 119, 84–95.

Mazaira, A., Konicek, P., 2015. Intense rockburst impacts in deep underground construction and their prevention. Can. Geotech. J. 52 (10), 1426–1439.

McGarr, A., 1976. Seismic moments and volume changes. J. Geophys. Res. Solid Earth 81 (8), 1487–1494.

Mendecki, A.J., 1997. Seismic Monitoring in Mines. Chapman Hall, London, UK.

Nateghi, R., 2011. Prediction of ground vibration level induced by blasting at different rock units. Int. J. Rock Mech. Min. Sci. 48 (6), 899–908.

Roy, M.P., Singh, P.K., Sarim, M., Shekhawat, L.S., 2016. Blast design and vibration control at an underground metal mine for the safety of surface structures. Int. J. Rock Mech. Min. Sci. 83, 107–115.

Sjöberg, J., Christiansson, R., Hudson, J.A., 2003. ISRM suggested methods for rock stress estimation - Part 2: overcoring methods. Int. J. Rock Mech. Min. Sci. 40 (7–8), 999–1010.

Snelling, P.E., Godin, L., McKinnon, S.D., 2013. The role of geologic structure and stress in triggering remote seismicity in Creighton mine, Sudbury, Canada. Int. J. Rock Mech. Min. Sci. 58, 166–179.

Tian, X., Song, Z., Wang, J., 2019. Study on the propagation law of tunnel blasting vibration in stratum and blasting vibration reduction technology. Soil Dynam. Earthq. Eng. 126, 105813.

Trifu, C.I., Shumila, V., 2010. Microseismic monitoring of a controlled collapse in field II at Ocnele Mari, Romania. Pure Appl. Geophys. 167 (1–2), 27–42.

Ulusay, R., Tuncay, E., Sonmez, H., Gokceoglu, C., 2004. An attenuation relationship based on Turkish strong motion data and iso-acceleration map of Turkey. Eng. Geol. 74 (3/4), 265–291.

Urbancic, T.I., Trifu, C.I., 2000. Recent advances in seismic monitoring technology at Canadian mines. J. Appl. Geophys. 45 (4), 225–237.

Wandycz, P., Święch, E., Eisner, L., Pasternacki, A., Wcisło, M., Maćkowski, T., 2019. Estimation of the quality factor based on the microseismicity recordings from Northern Poland. Acta Geophys. 67 (6), 2005–2014.

Wang, G.F., Gong, S.Y., Dou, L.M., Cai, W., Jin, F., Fan, C.J., 2019. Behaviour and bursting failure of roadways based on a pendulum impact test facility. Tunn. Undergr. Space Technol. 92, 103042.

Wanniarachchi, W.A.M., Ranjith, P.G., Perera, M.S.A., Rathnaweera, T.D., Lyu, Q., Mahanta, B., 2017. Assessment of dynamic material properties of intact rocks using seismic wave attenuation: an experimental study. R R. Soc. Open Sci. 4 (10), 170896.

Whitney, R., 2019. Quantifying near fault pulses using generalized Morse wavelets. J. Seismol. 23 (5), 1115–1140.

Wu, Y.K., Hao, H., Zhou, Y.X., 1998. Propagation characteristics of blast-induced shock waves in a jointed rock mass. Soil Dynam. Earthq. Eng. 17 (6), 407–412.

Wu, C., Lu, Y., Hao, H., 2004. Numerical prediction of blast-induced stress wave from large-scale underground explosion. Int. J. Numer. Anal. Methods GeoMech. 28 (1), 93–109.

Ye, G.X., Jiang, F.X., Guo, Y.H., Wang, C.W., 2008. Experimental research on seismic wave attenuation by field microseism monitoring in a deep coal mine. Chin. J. Rock Mech. Eng. 27, 1053–1058.

Zhou, J.R., Lu, W.B., Yan, P., Chen, M., Wang, G.H., 2016. Frequency-dependent attenuation of blasting vibration waves. Rock Mech. Rock Eng. 49 (10), 4061–4072.

Zhu, Z.M., Mohanty, B., Xie, H.P., 2007. Numerical investigation of blasting-induced crack initiation and propagation in rocks. Int. J. Rock Mech. Min. Sci. 44 (3), 412–424.

Jian Wu obtained his PhD degree in Civil Engineering from Wuhan University, China, in 2021. He is currently working as a postdoctoral fellow at PowerChina Huadong Engineering Corporation Limited, Hangzhou, China. His research interests include (1) experimental investigations on the propagation and attenuation characteristics of seismic wave; and (2) microseismic monitoring and warning of rockbursts in deep tunnels. He has been participated in several underground projects in China on rockburst risk and disaster assessment.